Applied Catalysis B: Environmental 337 (2023) 122946

Contents lists available at ScienceDirect

Applied Catalysis B: Environmental

journal homepage: www.elsevier.com/locate/apcatb

Reactive adsorption desulfurization of model FCC gasoline on Ni-based adsorbents: Effect of active phase dispersion on activity and HDS/HYD selectivity

A.A. Botin [a,b], R.E. Boldushevskii [a,b], A.V. Mozhaev [a,b], M. Ghambarian [c], M. Balar [c], M. Ghashghaee [d,*], P.A. Nikulshin [a,b,**]

[a] National University of Oil and Gas "Gubkin University", 65/1 Leninsky ave., Moscow 119991, Russia
[b] All-Russia Research Institute of Oil Refining, 6/1 Aviamotornaya st., Moscow 111116, Russia
[c] Gas Conversion Department, Faculty of Petrochemicals, Iran Polymer and Petrochemical Institute, P.O. Box 14975-112, Tehran, Iran
[d] Department of Petrochemical Synthesis, Faculty of Petrochemicals, Iran Polymer and Petrochemical Institute, P.O. Box 14975-112, Tehran, Iran

ARTICLE INFO

Keywords:
Reactive adsorption
Selective desulfurization
FCC gasoline
Nickel
Size effect
DFT calculations

ABSTRACT

A series of Ni/ZnO-Al_2O_3 and Ni/ZnO-SiO_2 adsorptive-catalytic adsorbents differing in the support composition (the Al_2O_3, SiO_2 and ZnO covered) and nickel surface content have been synthesized. Zinc oxide-based supports and Ni supported adsorbents were characterized using X-ray diffraction (XRD), temperature-programmed reduction (TPR), high-resolution transmission electron microscopy (HRTEM), X-ray photoelectron spectroscopy (XPS) and N_2 physisorption to study their structural properties and morphology. Desulfurization (HDS) and hydrogenation (HYD) activity of the synthesized systems, as well as the HDS/HYD selectivity factor (SF) were determined in the process of reactive adsorption of model FCC gasoline containing thiophene (1000 ppm of sulfur) and 1-hexene (20 wt%) on a fixed-bed flow-type laboratory unit. It has been established that an increase in the nickel surface content and average particle size of the active phase leads to an enhancement of the HDS/HYD selectivity factor regardless of the support used. The Ni/ZnO-SiO_2 sample with 8 at Ni/nm^2 exhibited the highest HDS/HYD selectivity at a high level of thiophene conversion (> 96%) in the chemisorption mode. The evolution of catalytic properties of Ni-Zn sorbents during FCC gasoline desulfurization process was estimated as well as characteristics of sulfurized samples. Relationships between the turnover frequency number in HDS and HYD reactions, HDS/HYD selectivity factor and size of Ni particles are discussed. DFT calculations of the adsorption thermodynamics were carried out for three model components and adsorption in the diffusion-controlled mode of the feedstock was studied for a series of nickel clusters. The results helped to explain the catalytic behavior of Ni-based sorbents in chemisorption and catalytic (after sulfur saturation) conditions.

1. Introduction

Over the past decades, hydroprocesses have played a dominant role in oil industry [1,2]. In order to meet new environmental standards and ever-increasing operational requirements for the quality of petroleum products, a great deal of research on hydrodesulfurization of crude oil is being done focused on two interrelated issues [3]. First, to obtain ultra-low sulfur fuels for automobiles and fuel cells, it is necessary to increase the desulfurization depth and, accordingly, activity of existing catalytic systems. On the other hand, for olefin-containing petroleum products, selectivity in desulfurization reactions with respect to hydrogenation reactions (HDS/HYD selectivity) should be increased to maintain the performance characteristics of petroleum products, such as the octane number of fluid catalytic cracking (FCC) gasoline.

Classical hydrotreatment processes have a number of disadvantages that do not allow solving these two problems at a time [4]. These are factors such as a high hydrogen pressure required to increase the desulfurization depth, which also reduces selectivity, a recombination of resulting hydrogen sulfide and olefins that form mercaptans in product steams, and high hydrogenation activity of the existing catalytic

* Corresponding author.
** Corresponding author at: National University of Oil and Gas "Gubkin University", 65/1 Leninsky ave., Moscow 119991, Russia.
E-mail addresses: m.ghashghaee@ippi.ac.ir (M. Ghashghaee), nikulshinpa@vniinp.rosneft.ru (P.A. Nikulshin).

https://doi.org/10.1016/j.apcatb.2023.122946
Received 12 February 2023; Received in revised form 28 May 2023; Accepted 31 May 2023
Available online 7 June 2023

systems. In this regard, many studies devoted to alternative processes of desulfurization of the olefin-containing feedstock are underway [5–7]. The most interesting and promising of them, in our opinion, is reactive adsorption (RADS) of sulfur compounds [8].

The essence of this process is desulfurization of various hydrocarbon media on bifunctional adsorptive catalytic systems, among which the most widely used are Ni-ZnO formulations [9]. The mechanism of this process is quite well studied and includes two main stages [10–12]. Firstly, the sulfur compound is destroyed to form hydrocarbon and hydrogen sulfide, which is absorbed by nickel to give nickel sulfide. The second component, zinc oxide, then regenerates nickel by absorbing sulfur to form zinc sulfide. Thus, maintaining nickel in the active phase throughout the entire adsorptive catalytic cycle enables a desulfurization rate of more than 99.9% with a high sorbent capacity [13].

However, significant hydrogenation of olefins occurs on classical Ni-ZnO bimetallic adsorptive catalytic systems [14,15], which is why many studies are aimed at finding ways to preserve the octane number of the product. It has been shown that HDS/HYD selectivity can be improved by 'poisoning' the active phase with an alkaline earth metal or by replacing nickel with copper [16,17]. The authors also suggest changing the composition of the support to partially aromatize raw materials with a view to maintain the octane number of the product [18].

It is known that activity of bimetallic reactive adsorption sorbents is positively affected by high dispersion of active phase particles, high Lewis acidity, and weak metal-support interaction [19,20]. However, no direct structure-property correlations were revealed, and the dispersion of the active phase particles was estimated only indirectly. The influence of various factors on HDS/HYD selectivity of RADS systems had also not been systematically studied before. Nevertheless, size effect of active phase particles is a key characteristic for other classic hydrodesulfurization catalysts. For CoMo-systems [8,21] it has been found that both an increase in the linear size of MoS_2 crystallites, as well as an increase in the average stacking number, leads to an increase in the HDS/HYD selectivity of the FCC desulfurization process. However, NiS-based systems have not been studied in this way. In turn, FCC gasoline RADS is a new process for which analogous effects have not been fundamentally studied. We have only shown that for Ni/ZnO-Al_2O_3 sorbents there is no direct effect of zinc oxide present on the surface [22] and the surface content of nickel [23] on HDS/HYD selectivity of the desulfurization process of the olefin-containing feedstock. This study is focused on the influence of the Ni active phase characteristics and support composition (Al_2O_3 or SiO_2 and ZnO modified) on activity and HDS/HYD selectivity in desulfurization of model FCC gasoline. The size effect considered by us is also inherent in other FCC desulfurization catalysts, however, for Ni(Zn) systems of the RADS process, it describes for the first time. In addition, the evolution of catalytic properties of nickel-zinc systems during desulfurization as well as the effect of dispersion and characteristics of the active phase on the HDS/HYD selectivity of the sulfided Ni-Zn catalyst were not considered earlier. Study of changes in the composition of particles of the active phase and comparison of HDS/HYD selectivity before and after sulfurization in feed stream will make it possible to determine how to control HDS/HYD selectivity and create sorbents or catalytic materials with the required properties. Therefore, we considered it more useful to study not only the chemisorption regime of the desulfurization process but also the catalytic properties of the sorbents and their characteristics after sulfurization in feed stream. In parallel with the experiment, DFT calculations of adsorption parameters of the studied feedstock components (thiophene and 1-hexene) on the surface of nickel particles were carried out to explain the obtained results.

2. Experimental

2.1. Preparation of supports and adsorbents

γ-Alumina (Bayer), silica, γ-alumina and silica with 25% wt. zinc oxide (designated as "ZnO-Al_2O_3" and "ZnO-SiO_2", respectively) were used as supports. ZnO-Al_2O_3 and ZnO-SiO_2 supports were prepared by wetness impregnation of Al_2O_3 with zinc nitrate solution (Lenreactiv, 98.1%) followed by drying at 120 °C and calcination at 550 °C.

Ni/ZnO-Al_2O_3 and Ni/ZnO-SiO_2 adsorbents were prepared by wetness impregnation of the supports with nickel nitrate solution (Lenreactiv, 99.2%) followed by drying at 120 °C and calcination at 500 °C. Three adsorptive catalytic systems with surface concentrations of nickel atoms 2, 6 and 8 Ni at/nm^2 were prepared for each support.

2.2. Characterization of adsorbents

Specific surface area and pore size distribution for supports and adsorbents were determined by a nitrogen porosimeter on a Quantachrome Nova 1200e. Using the multipoint Brunauer-Emmet-Teller (MBET) method and the Barret-Joyner-Halenda (BJH) method, the specific surface area and average pore diameter were determined. The samples were dried in vacuum ($P < 10^{-1}$ Pa) at 120 °C for 4 h before testing.

The elemental composition of the samples was determined on an iCAP 6500 inductively coupled plasma atomic emission spectrometer.

The temperature-programmed reduction (TPR) curves were recorded on a USGA-101 M analyzer in the temperature range from 40° to 900°C. Before TPR studies, the adsorbents were dried in a nitrogen flow at a temperature of 200 °C for 2 h.

Prior to XRD, XPS and TEM studies, the adsorbents were reduced in a hydrogen flow at a temperature of 400 °C for 4 h. All manipulations with samples after reducing were carried out in a glove box under an argon atmosphere to prevent oxidation of the surface of the samples.

The diffraction patterns of the samples were obtained on a DRON-3 X-ray diffractometer with a monochromatic radiation source Cu Kα = 0.154 nm.

Average particle size of the active phase and distribution were established by processing the TEM micrographs of the surface of adsorptive catalytic samples made on a Tecnai G2 30 transmission electron microscope with a LaB6 cathode at an acceleration voltage of 200 kV. Based on average particle size data (more than 500 were processed for each sample), dispersion was calculated using the formula [24]:

$$D = \frac{6A}{\rho d N_a S_a} \times 1000 \quad (1)$$

where A is the atomic mass of nickel, g/mol; ρ is the density, g/cm^3; d is the average particle size, nm; N_a is the Avogadro number, mol^{-1}; S_a is the area occupied by the atom on the surface, m^2.

The electronic state of nickel on the sample surface was studied by X-ray photoelectron spectroscopy (XPS) on an Axis Ultra DLD spectrometer from Kratos using AlK_a (hν=1486.6 eV). The binding energy scale (E_b) was preliminarily calibrated according to the position of the peaks of the main levels Au4f$_{7/2}$ (84.0 eV) and Cu2p$_{3/2}$ (932.67 eV). The samples were applied on double-sided conductive adhesive tape. The recharging effect arising in the process of electron photoemission was minimized by irradiating the sample surface with slow electrons using a special source (flood gun). The C1s line (284.8 eV) from carbon present on the catalyst surface was used for calibration.

2.3. Density functional theory (DFT) calculations

Monatomic and sub-nanometric particles of nickel (Ni$_x$) and nickel sulfide (Ni$_x$S) were optimized at the molecular level (x = 1–7) to approach single-atom catalysis and aggregated nickel sites for both pure and sulfided catalysts. The optimization method involved M06 with LANL2DZ for Ni and SVP for S, C, and H atoms [25–27]. The energetic data for all structures were obtained at M06/TZVP. The method was verified based on the structural parameters of the Ni_2 dimer and free thiophene [28–30]. As shown in Table 1, good agreement was found

Table 1
Selected bond length and vibrational frequency data for the Ni_2 dimer and free thiophene molecule.

Parameter	d_{Ni-Ni} (Å)	ω_{Ni2} (cm^{-1})	d_{C-C} (Å)	d_{C-S} (Å)
This work	2.08	381.1	1.37, 1.42	1.72
Literature	2.09[a]	381[b]	1.370[c], 1.423[c]	1.714[c]

[a] [28]
[b] [29]
[c] [30]

between the calculated and experimental values.

Density functional theory (DFT) computations were implemented using NWChem 6.5 [31]. Mercury 3.6 [32] was used to create the pictorial outputs. After optimizing the pure and sulfided nickel substrates, thiophene (C_4H_4S), 1-hexene (C_6H_{12}), and n-heptane (C_7H_{16}) molecules were adsorbed on the obtained clusters to identify thermodynamically plausible adsorption configurations. Bader charges were calculated based on the quantum theory of atoms in molecules (QTAIM) [33] at M06/TZVP, with the electronic wave function analysis carried out in Multiwfn 3.8 [34].

2.4. Reactive adsorption desulfurization of model FCC gasoline

Activity and HDS/HYD selectivity in desulfurization of model FCC gasoline were carried out on a laboratory flow unit with a fixed catalyst bed. The desulfurization tests were performed at a temperature of 400 °C, a pressure of 0.5 MPa, a weight hourly space velocity (WHSV) of 5.2 h^{-1} and an H_2/feedstock ratio of 100 Nm^3/m^3 of the feedstock. The synthesized adsorbents were loaded in the form of 0.2–0.5 mm fractions in a mixture with an inert material (corundum) in a volume ratio of 1:1 in the amount of 0.86 g. Before testing, all loaded samples were activated by *in situ* reduction in the same laboratory bench reactor in a hydrogen flow at a temperature of 400 °C and a pressure of 2 MPa for 4 h.

The model feedstock used for testing has the following composition (% wt.): n-heptane (EKOS-1, 99.8%) – 43.7%; toluene (EKOS-1, 99.8%) – 35.0%; 1-hexene (Nizhnekamskneftekhim, 98.0%) – 20.0%; thiophene (Sigma-Aldrich, 99.0%) – 0.26%, 1000 ppm of sulfur; n-octane (EKOS-1, 98.5%) – 1.0%, internal standard. All reagents were used without additional purification.

The content of thiophene and olefins in the desulfurization products of the model feedstock was determined on a gas chromatograph "Kristalluks-400 M" with a flame ionization detector equipped with a ZB-1 30 m × 0.25 mm capillary column. The analysis was carried out by programming the temperature of the column from 0° to 250°C; the carrier gas flow rate was 1 cm^3/min.

Conversion values of thiophene and olefins were calculated using Eqs. (2) and (3), respectively:

$$HDS(\%) = \frac{C_T^0 - C_T}{C_T^0} \times 100 \quad (2)$$

$$HYD(\%) = \frac{C_O^0 - C_O}{C_O^0} \times 100 \quad (3)$$

where C_T^0 and C_O^0 are the content of thiophene and olefins in the feedstock (% wt.), respectively; C_T and C_O are the content of thiophene and olefins in the products (% wt.), respectively.

Two stages of the desulfurization process were evaluated: the chemisorption stage first and the catalytic stage second. The chemisorption stage, corresponding to the beginning of the experiment, was characterized by a high stable level of conversions and absence of hydrogen sulfide in the product mixture, which was determined using indicator tubes. Duration of chemisorption stage was estimated for each sample as a stable HDS time at the beginning of the experiment. The catalytic stage was characterized by constant values of thiophene and olefin conversion at the end of the test; the calculation took into account the last 4 h of the experiment. To evaluate HDS and HYD performances of sorbents at the stage of chemisorption and catalysis, the average values determined as the arithmetic mean were used.

The HDS/HYD selectivity factor of the studied adsorbents was determined as follows [35]:

$$SF = \frac{\ln(1 - HDS)}{\ln(1 - HYD)} \quad (4)$$

where HDS and HYD are conversion values of thiophene and olefins, respectively.

The turnover frequencies (TOF) number for thiophene and 1-hexene molecules was determined using Eqs. (5) and (6), respectively:

$$TOF_T = \frac{F_T \bullet HDS}{\frac{m_{Ni}}{Ar} \bullet \left(\frac{1}{L}\right) \bullet \frac{\%Ni^0_{XPS}}{100\%}} \quad (5)$$

$$TOF_H = \frac{F_H \bullet HYD}{\frac{m_{Ni}}{Ar} \bullet \left(\frac{1}{L}\right) \bullet \frac{\%Ni^0_{XPS}}{100\%}} \quad (6)$$

where F_T and F_H are molar flow of thiophene and olefins (mol/h), respectively, HDS and HYD are conversion values of thiophene and olefins (%), respectively, m_{Ni} is total nickel mass in the sample (g), Ar is nickel atomic mass (g/mol), L is average particle size of the active phase from the TEM analysis (nm), $\%Ni^0_{XPS}$ is the surface metallic nickel fraction from the XPS analysis (% rel.).

3. Results and discussion

3.1. Characterization of adsorptive catalytic systems

The characteristics of the supports are summarized in Table 2. The N_2 adsorption–desorption isotherms and pore size distribution curves of supports are shown in Figs. S1 and S2.

Where zinc oxide was added to the silica and alumina surface, a decrease in the surface area and pore volume of the support and an increase in the average pore size were observed. In this case, a greater increase in the average pore diameter was observed for alumina than for silica. As seen from pore size distribution data (Fig. S2), alumina has a generous portion of pores 5–7 nm in diameter. Apparently, where zinc oxide was added, the pores were filled completely, which led to the increase in the average pore diameter of the ZnO-Al_2O_3 composite. The zinc oxide mass fraction determined in the composition of the synthesized supports was close to the amount planned to be added (25% wt.).

The increase in the mass fraction of nickel in the prepared adsorbents led to the decrease in the surface area and pore volume, while the average pore diameter changed in different ways (Table 3). The increase in the average pore diameter can be explained by a similar effect observed when zinc oxide was added.

Worth noting is the effect of zinc oxide present in the support on the TPR results (Figs. S3–S6). A comparison of reduction temperatures of the active phase of Al_2O_3-based samples containing and not containing zinc oxide shows that temperatures of the maximum reduction rate are close

Table 2
Support characteristics.

Support	Surface area (m^2/g)	Average pore diameter (nm)	Pore volume (cm^3/g)	ZnO content (% wt.)
Al_2O_3	276	6.1	0.80	-
SiO_2	356	8.7	1.50	-
ZnO-Al_2O_3	151	11.5	0.51	23.7
ZnO-SiO_2	225	9.4	0.67	24.1

Table 3
Characteristics of the prepared adsorbents.

Adsorbent	Ni content (% wt.)	Surface area (m^2/g)	Average pore diameter (nm)	Pore volume (cm^3/g)	TPR peak maximum[a] (°C)
2-Ni/Al_2O_3	5.1	275	6.5	0.76	634 ± 11/ 776 ± 10
6-Ni/Al_2O_3	13.4	212	6.1	0.66	523 ± 7/ 614 ± 16
8-Ni/Al_2O_3	16.9	173	6.1	0.56	539 ± 15
2-Ni/SiO_2	6.4	318	9.5	0.92	400 ± 12
6-Ni/SiO_2	16.5	258	9.3	0.65	407 ± 7
8-Ni/SiO_2	20.5	237	11.8	0.63	403 ± 8
2-Ni/ZnO-Al_2O_3	2.8	129	8.6	0.51	645 ± 14
6-Ni/ZnO-Al_2O_3	7.9	125	10.3	0.46	595 ± 12
8-Ni/ZnO-Al_2O_3	10.2	113	11.3	0.42	592 ± 11
2-Ni/ZnO-SiO_2	4.2	200	9.5	0.61	480 ± 8/ 638 ± 9
6-Ni/ZnO-SiO_2	11.3	182	9.4	0.52	509 ± 8/ 651 ± 12
8-Ni/ZnO-SiO_2	14.1	177	8.6	0.49	510 ± 10/ 635 ± 14

[a] average values from several measurements

to each other (Figs. S3-S4) indicating a weak influence of zinc oxide. At the same time, for the SiO_2-based systems (Table 3), when zinc oxide is added, there are two peaks on the TPR curves: a small low-temperature one (480–510 °C) and a more intense high-temperature one (635–651 °C). The first peak corresponds to the reduction of surface nickel atoms. The high temperature peak corresponds to the reduction of the subsurface nickel, which shifts to the high-temperature region due to the Ni-Zn strong interaction. Presumably, this effect has not been detected for the Al_2O_3-based systems because of the preferred interaction of ZnO with alumina acidic sites.

The X-ray diffraction patterns of the pre-reduces samples (Figs. 1–4) confirmed these transformations. In the case of Al_2O_3-based adsorbents, nickel phases were found only for the samples with high surface concentrations and were represented primarily by nickel oxide species. The presence of metallic nickel in the 8-Ni/Al_2O_3 sample can be explained by a large mass fraction of nickel that led to the formation of large particles less bound to the support. Also of note are intense reflections of the $ZnAl_2O_4$ (Fig. 2) phase which indicate a high degree of its crystallinity.

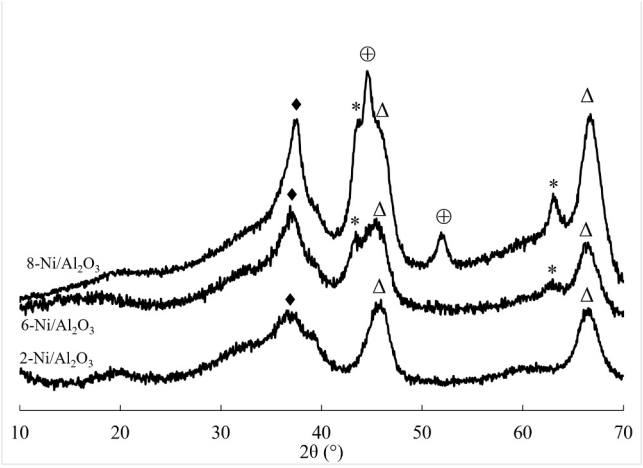

Fig. 1. XRD patterns of reduced Al_2O_3-based samples. * – NiO (PDF 78–0429), Δ – γ-Al_2O_3 (PDF 29–0063), ◆ – $NiAl_2O_4$ (PDF 65–3102), ⊕ – Ni (PDF 04–0850).

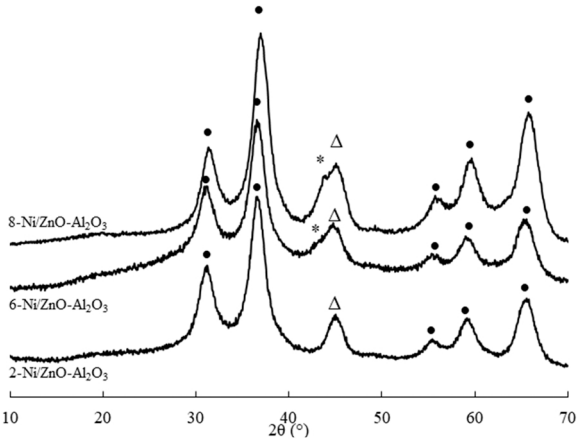

Fig. 2. XRD patterns of reduced ZnO-Al_2O_3-based systems. * – NiO (PDF 78–0429), Δ – γ-Al_2O_3 (PDF 29–0063), • – $ZnAl_2O_4$ (PDF 82–1043).

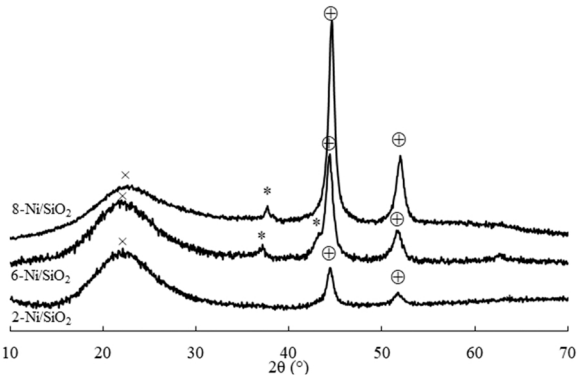

Fig. 3. XRD patterns of reduced SiO_2-based systems. ⊕ – Ni (PDF 04–0850), * – NiO (PDF 78–0429), × – SiO_2 (PDF 85–1565).

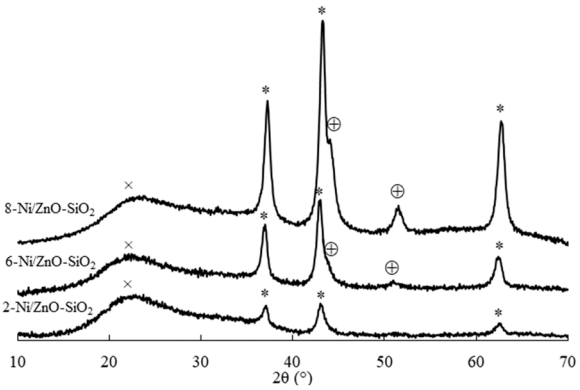

Fig. 4. XRD patterns of reduced ZnO-SiO_2-based systems. ⊕ – Ni (PDF 04–0850), * – NiO (PDF 78–0429), × – SiO_2 (PDF 85–1565).

The formation of this phase seems to prevent the ZnO influence on the behavior of Ni particles.

The XRD results for SiO_2 and ZnO-SiO_2 supported samples indicate the effect of zinc oxide on nickel reduction (Figs. 3–4). For SiO_2-based samples, the metallic nickel phase is the most crystalline, whereas in ZnO-SiO_2 samples two phases were identified with oxide nickel phase predominating. Zinc-containing phases were not found in these samples, which may be indicative of their low crystallinity and good interaction with NiO species.

XPS results for the samples (Fig. 5, Table S1 and Table 4) also

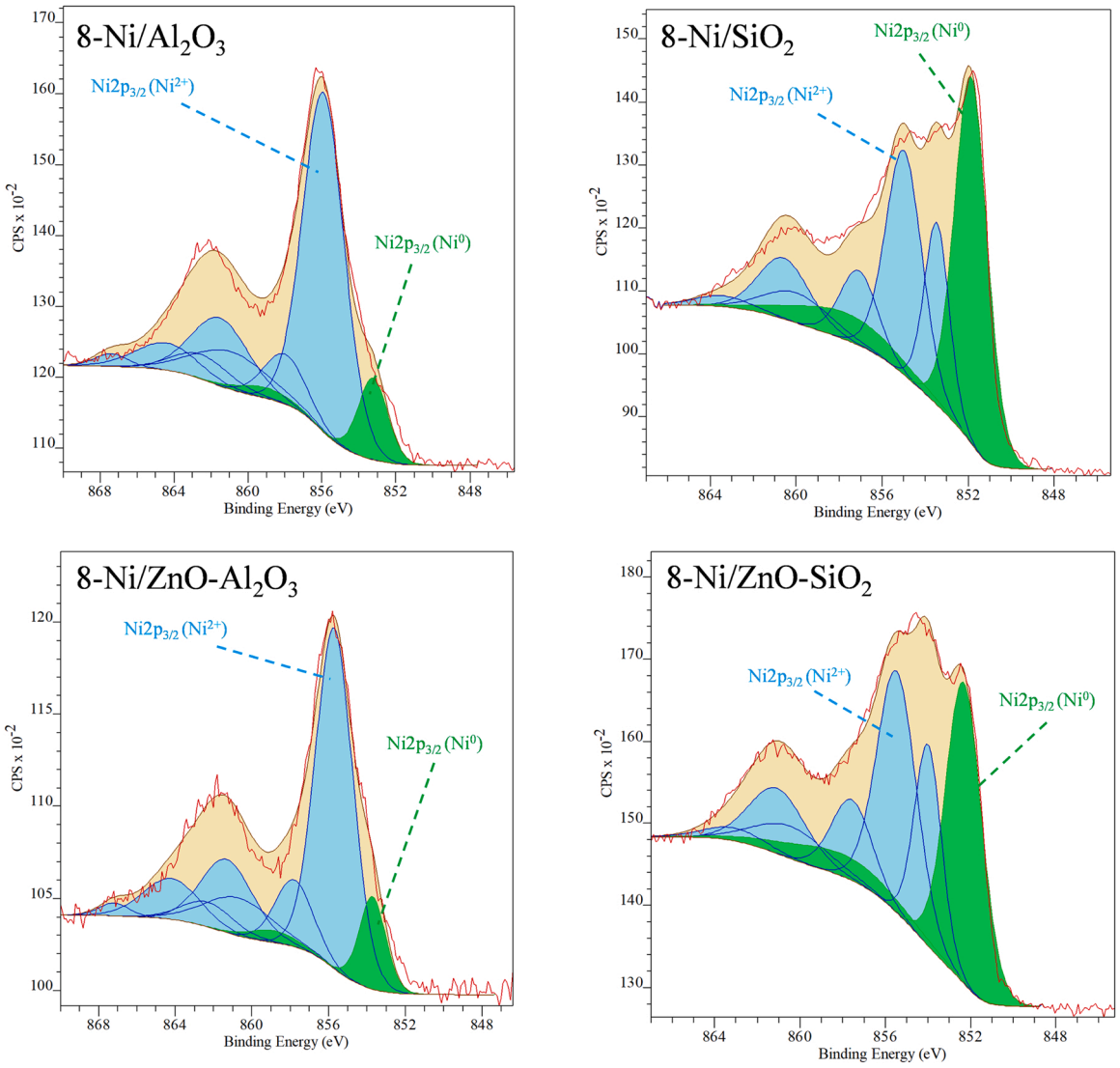

Fig. 5. XPS spectra of the reduced samples.

Table 4
Ni amount in the metal state and particle dispersion found from XPS and TEM data.

Adsorbent	Ni^0 amount on the surface from XPS (%)	Average particle size from TEM (nm)	Dispersion (%)
2-Ni/Al_2O_3	1.3	4.8	21.0
6-Ni/Al_2O_3	5.8	6.2	16.3
8-Ni/Al_2O_3	9.9	6.4	15.8
2-Ni/ZnO-Al_2O_3	2.2	4.4	22.9
6-Ni/ZnO-Al_2O_3	5.3	5.1	19.8
8-Ni/ZnO-Al_2O_3	10.4	5.2	19.4
2-Ni/SiO_2	34.9	10.2	9.8
6-Ni/SiO_2	49.5	11.0	9.2
8-Ni/SiO_2	41.1	11.6	8.7
2-Ni/ZnO-SiO_2	29.8	5.4	18.5
6-Ni/ZnO-SiO_2	35.2	6.8	14.7
8-Ni/ZnO-SiO_2	34.6	8.4	12.0

indicate the influence of the support's nature on the state of surface atoms. In the studied samples, surficial Ni atoms were in several electronic states (Fig. 5). Apart from the metallic form of nickel, oxidized nickel was identified in the samples. For Al_2O_3-based systems, it can be seen that only a small fraction of surface nickel atoms (1.3 – 10.4%) transformed into the metallic species when being reduced at a temperature of 400 °C, which is in line with the TPR results. This confirms a significant interaction occurring between the active phase and the support, which prevented nickel reduction to the metallic species. The presence of zinc oxide slightly increased the metallic nickel proportion on the sample surface. However, oxide nickel remained the predominant species. For SiO_2-based systems, a significant fraction of surface nickel atoms was in the reduced state (29.8–49.5%). Zinc oxide present in the samples decreased the metallic nickel proportion and increased the nickel oxide proportion. For alumina-based samples, this effect has not been found since zinc was strongly bound to Al_2O_3, which was confirmed by the XRD results. For Ni/ZnO-SiO_2-systems, the predominant surface nickel species was oxide, which agrees with the XRD results.

In the HRTEM micrographs (Fig. 6), active phase particles in the form of dark spots were found for all studied samples. In the maximum magnification images, it was possible to detect lattice fringes and calculate interplanar distances for fixed crystallites. Interplanar

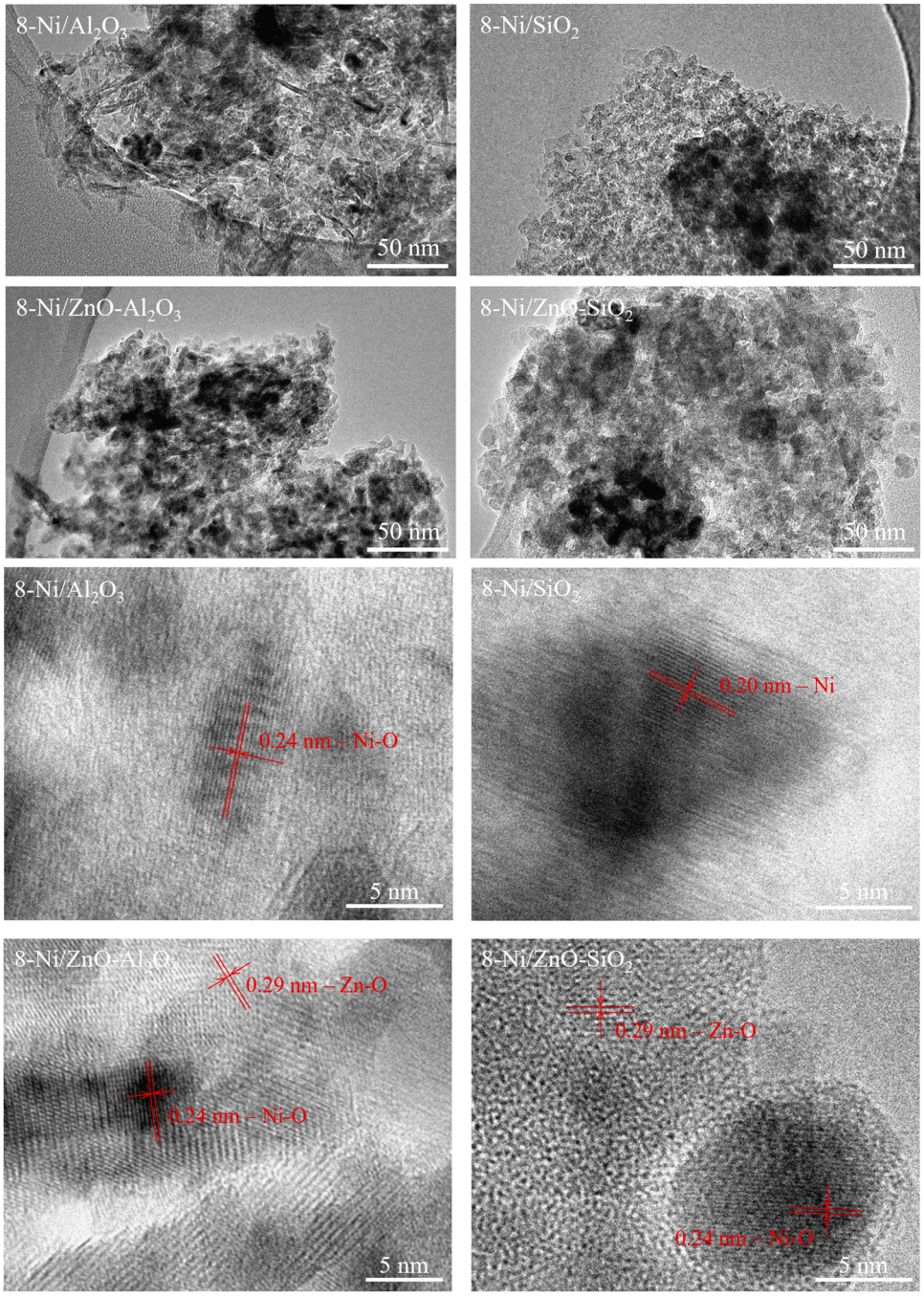

Fig. 6. HRTEM micrographs of the reduced samples.

distances corresponding to the oxide nickel species (0.24 nm) were recorded for all samples; however, particles with the 0.2 nm interplanar distance predominated in the Ni/SiO_2 samples, which corresponds to the metallic Ni species. Moreover, lattice fringes were found with 0.29 nm interplanar distance typical for the ZnO form. In the case of Al_2O_3 samples, these structures were more clearly visible than in the case of SiO_2 samples, which is in agreement with the XRD results.

Measurements of Ni average particle size of the active phase (Table 4) show that, in almost all cases, increasing the Ni surface concentration led to the increase in particle size. In addition, Ni average particle size for the SiO_2 systems (5.4–11.0 nm) significantly exceeds average particle size for the Al_2O_3 systems. The reasons for these differences lie in different metal-support interactions and their change after ZnO modification.

XRD results (Fig. 1) show a strong interaction between nickel and alumina resulting in the formation of mixed oxides ($NiAl_2O_4$), whereas silica is inert towards nickel. This difference was indicated both by a shift of the TPR peak by 120 – 230 °C (Table 2) and by a significantly larger proportion of metallic nickel on the surface of reduced SiO_2 supported samples determined by XPS. It is exactly this effect that, in our opinion, leads to a twofold difference in dispersion of nickel particles on pure silica and on alumina.

The zinc oxide effect on dispersion of Ni particles for the ZnO-SiO_2 support is beneficial. TPR showed the presence of a strong metal interaction in Ni/ZnO-SiO_2 systems which could prevent the nickel agglomeration over the surface due to the formation of Ni-Zn mixed oxides and the increase in particle dispersion after reduction. An interesting fact is that zinc oxide not only increased dispersion of Ni particles

for the 2-Ni/ZnO-SiO_2 sorbent, but also maintained it at higher Ni loading. For SiO_2 systems, when the Ni surface concentration was increased from 2 to 8 at/nm^2, a decrease in nickel dispersion (from 9.8% to 8.7%) was observed, whereas for ZnO-SiO_2 systems the change was much more significant (from 18.5% to 12.0%). This is probably due to a change in the Ni:Zn ratio associated with the increase in nickel loading, which led to the increase in the number of atoms unbound to zinc, reduced the degree of interaction between the active phase and the support, and increased nickel dispersion.

For Al_2O_3 systems, the introduction of zinc oxide resulted in a less significant increase in Ni particles dispersion. Apparently, this is due to interaction between alumina active sites and zinc oxide, confirmed by XRD results, so the influence of zinc oxide was not as noticeable as in the case of silica.

3.2. Results of adsorptive-catalytic tests

3.2.1. HDS and HYD performances of adsorbents

A study on desulfurizing activity and HDS/HYD selectivity was carried out on the model feedstock for all synthesized adsorbents. It should be noted that in addition to thiophene, no other sulfur compounds were found in the products. As can be seen from the dynamics of changes in conversions of thiophene and olefins, and HDS/HYD SF during the test (Figs. 7–8, Figs. S7-S13), all samples exhibited desulfurizing activity that decreased from the beginning (chemisorption stage) to the end of the experiment after sulfur saturation from the feed (catalytic stage). However, it should be noted that all samples also had a similar trend in hydrogenation activity with respect to olefins.

Average thiophene and olefin conversion values, as well as the results of HDS/HYD selectivity factor calculations are presented in Table 5. The increase in the surface concentration of nickel, as seen from the experimental results, increased significantly both HDS and HYD activities at the chemisorption stage for both types of supports (Fig. 9). At the same time, Al_2O_3-based systems with higher active phase dispersion than those SiO_2 supported exhibited higher HDS activity (excluding 8-Ni/SiO_2) at the chemisorption stage. However, if the ZnO-SiO_2 and ZnO-Al_2O_3 systems are taken into account, there are no relationships between the desulfurization activity and dispersion of active phase particles. This can be explained by the multidirectional effect of dispersion and the metals-support interaction on the desulfurization activity. On the one hand, a number of scientific groups have shown [19, 20] that the high dispersion of the active phase provides a high desulfurizing activity. Higher dispersion in this study was determined for systems supported by Al_2O_3. On the other hand, it has been reported [36, 37] that in order to provide a high desulfurization activity, it is

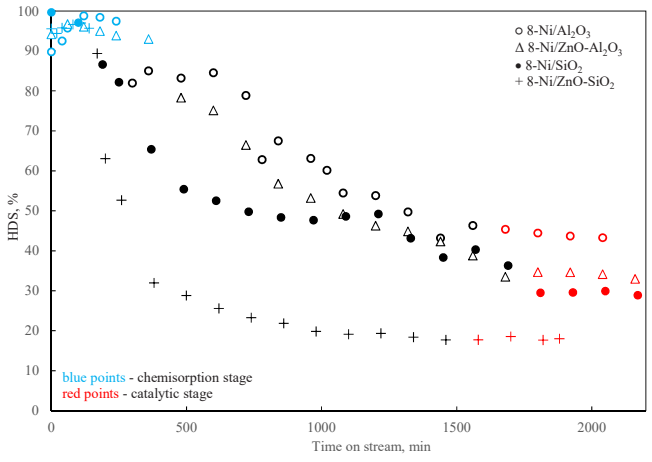

Fig. 7. HDS activity of (ZnO)-Al_2O_3 and -SiO_2 supported sorbents with Ni loading 8 at/nm^2.

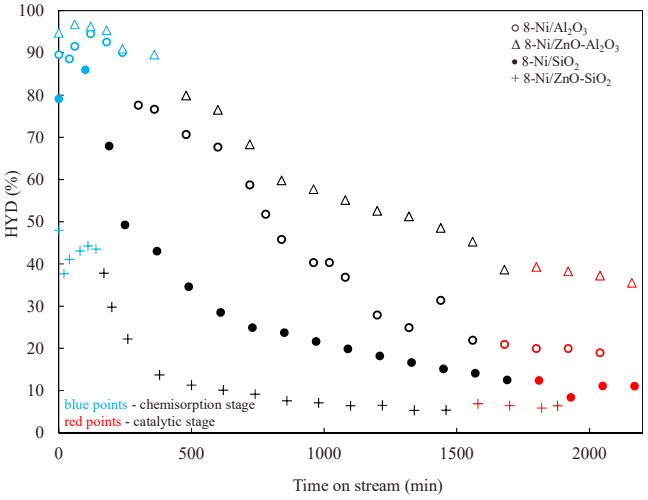

Fig. 8. HYD activity of (ZnO)-Al_2O_3 and -SiO_2 supported sorbents with Ni loading 8 at/nm^2.

Table 5
Performance of the prepared adsorptive-catalytic samples.

Adsorbent	Chemisorption regime				Catalytic regime		
	Capacity (mg_S/g_{Ads})	HDS[a] (%)	HYD[a] (%)	SF	HDS[a] (%)	HYD[a] (%)	SF
2-Ni/Al_2O_3	1.1	83.1	77.7	1.18	33.7	20.8	1.76
6-Ni/Al_2O_3	13.6	96.7	89.8	1.49	40.1	18.8	2.46
8-Ni/Al_2O_3	22.1	96.6	91.5	1.37	44.2	20.0	2.61
2-Ni/ZnO-Al_2O_3	1.9	84.4	86.9	0.91	27.9	36.5	0.72
6-Ni/ZnO-Al_2O_3	28.9	94.2	93.4	1.05	48.9	54.8	0.85
8-Ni/ZnO-Al_2O_3	30.3	95.5	95.8	0.98	33.6	36.4	0.90
2-Ni/SiO_2	1.6	69.5	59.5	1.31	12.0	7.1	1.74
6-Ni/SiO_2	7.8	90.4	75.7	1.66	28.3	11.2	2.80
8-Ni/SiO_2	11.7	98.4	82.5	2.37	29.5	10.8	3.06
2-Ni/ZnO-SiO_2	1.8	89.6	58.0	2.61	17.0	8.6	2.07
6-Ni/ZnO-SiO_2	13.3	93.5	54.6	3.46	40.1	21.0	2.17
8-Ni/ZnO-SiO_2	15.5	95.8	42.9	5.66	17.9	6.4	2.98

[a] average values on the regime

necessary to reduce the interaction between the metals (Ni and Zn) and the support. From the results of adsorbents characterization, it can be seen that the systems supported on SiO_2 are characterized by a lower degree of interaction between the active phase and the support than systems supported by Al_2O_3. Therefore, we observe a comparable conversion of thiophene for systems supported by SiO_2 and Al_2O_3.

The expected result is the increase in the sulfur capacity associated with the increase in the surface concentration of nickel and with the presence of zinc oxide in the samples. However, it should be noted that Al_2O_3 and ZnO-Al_2O_3-based systems with 6 and 8 at/nm^2 Ni surface loading had a higher sulfur capacity than SiO_2 supported ones. Also, for the best systems, the degree of sulfurization at the chemisorption stage was estimated (the ratio of the experimentally obtained capacity to the theoretically possible value, considering Ni_3S_2 and ZnS as fully sulfided phases). It was found that 6-Ni/ZnO-Al_2O_3 and 8-ZnO-Al_2O_3 systems had a high degree of sulfurization (24–25%), while for 6-Ni/ZnO-SiO_2 and 8-Ni/ZnO-SiO_2 systems the degree of sulfurization reduced to

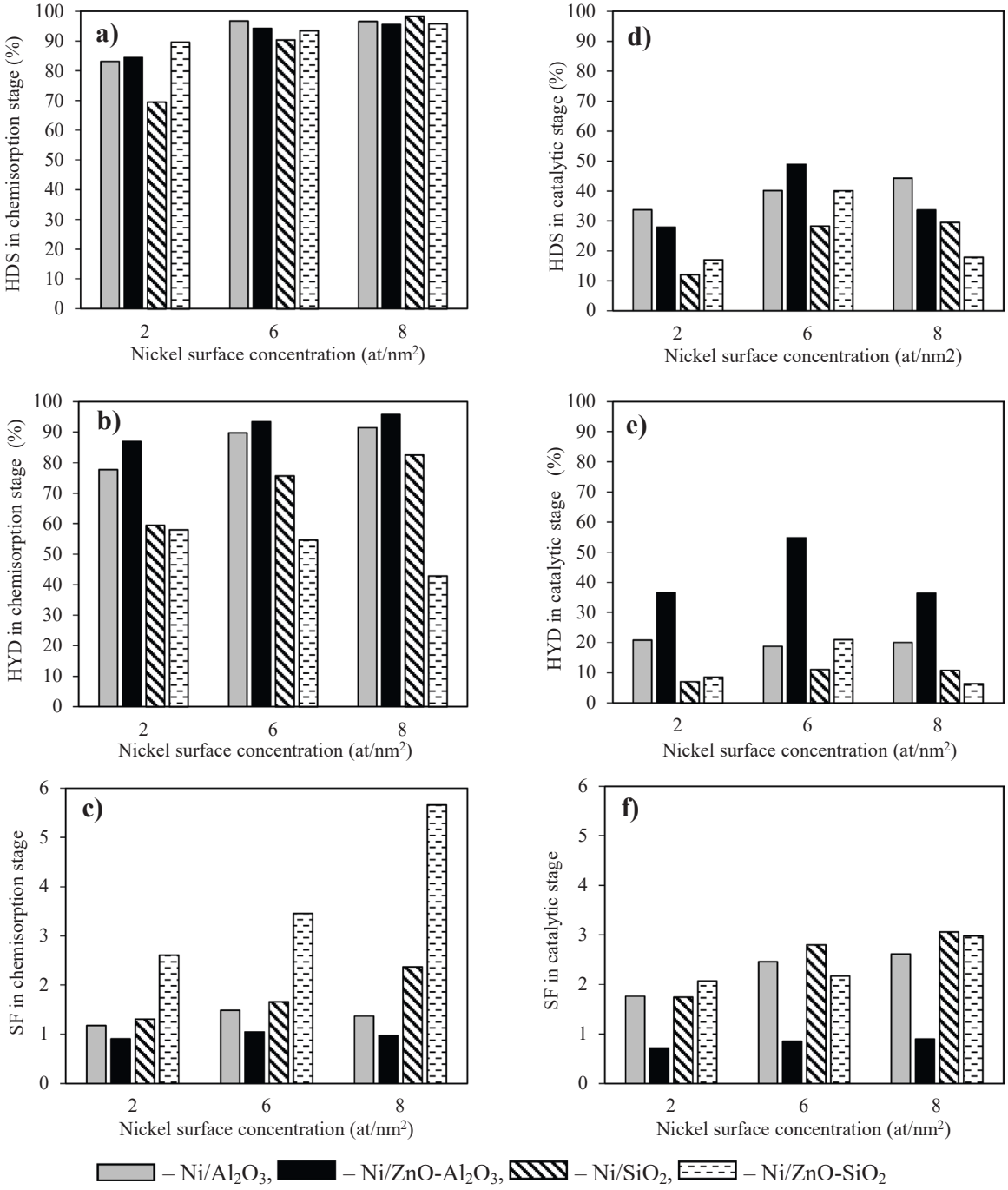

Fig. 9. Efficiency of the prepared adsorptive-catalytic samples. a) HDS in the chemisorption stage; b) HYD in the chemisorption stage; c) SF in the chemisorption stage; d) HDS in the catalytic stage; e) HYD in the catalytic stage; f) SF in the catalytic stage.

11–12%. This is an interesting result, since the XRD and XPS showed that nickel and zinc are strongly bound to the Al_2O_3 support, while they are unbound on the SiO_2 surface. Apparently, the formation of $NiAl_2O_4$ and $ZnAl_2O_4$ does not prevent deep sulfurization of metals. The low sulfur capacity of the systems supported by silica, on the basis of this, is explained by the low dispersity of the active phase. This is consistent with the results of other studies [20], which showed a positive effect of the dispersion of the active phase on the sulfur capacity of sorbents. At the same time, it is impossible to explain the low capacity for Ni/ZnO-SiO_2 systems by the effect of dispersion of the active phase. The study of spent sorbents, which is described below, allowed shedding light on this phenomenon.

3.2.2. *HDS/HYD selectivity of adsorbents*

HDS/HYD selectivity of Al_2O_3-based systems at the chemisorption stage was lower than that of SiO_2 supported systems, of which the most selective were 8-Ni/SiO_2 and Ni/ZnO-SiO_2 samples with the HDS/HYD selectivity factor higher than 2 (Fig. 9). Since the desulfurization activity of these systems is comparable, the increased selectivity of Ni/ZnO-SiO_2–systems is due to a significant decrease in the hydrogenating activity.

Of interest is the effect of zinc oxide on HDS/HYD selectivity of systems at the chemisorption stage. For Al_2O_3-based systems, the presence of zinc oxide slightly decreased HDS/HYD selectivity correlated with enhancing dispersion of Ni particles. The reverse situation was observed for SiO_2-based systems. The 8-Ni/ZnO-SiO_2 system showed the

best HDS/HYD selectivity at the chemisorption stage (SF=5.66) due to a drop in hydrogenation activity. During the chemisorption stage, HDS/HYD selectivity of the ZnO-SiO_2 supported sorbents increased significantly with Ni loading compared to pure SiO_2 supported sorbents. Adding ZnO to SiO_2 entailed the increase in Ni particle dispersion, yet HDS/HYD selectivity of the process also increased. Based on TPR, XRD and XPS data, a significant effect of zinc oxide on the chemical and electronic state of nickel was established, which was expressed in the increase in the nickel reduction temperature and the predominance of oxide crystallites over metal ones in the volume of active phase particles. Apparently, this effect makes a more significant contribution to HYD activity of the samples and HDS/HYD selectivity of the process than nickel dispersion.

For all studied systems, sulfurization during chemisorption led to the decrease in HYD and HDS activity in the stage of catalysis, however, a significant effect of zinc oxide on the change in selectivity was still observed. For all zinc oxide-free samples, the increase in the HDS/HYD selectivity factor after sulfurization of the sorbent was detected, which could be due to lower HYD activity of nickel sulfide in relation to metal. However, in the presence of zinc oxide, the HDS/HYD selectivity factor of the process decreased after sulfur saturation of the samples. Since the study of the chemisorption stage showed a significant effect of zinc on the RADS process parameters, it can be assumed that due to interaction with zinc some of nickel atoms remained in a more active state, which increased HYD activity of the samples relative to desulfurizing activity.

3.2.3. Characterization of spent adsorbents

The reflections corresponding to the zinc sulfide phase were found in the diffraction patterns of the samples (Fig. 10). This confirms the autoregeneration process, which is the basis of the RADS mechanism. In addition, the diffraction pattern of the 8-Ni/ZnO-SiO_2 sample contains an intensive reflection in the region of 42.5° – 44.0°. This reflection does not correspond to the NiO phase, since there is no other intensive reflection of this phase in the region of 61.8° – 63.5°. We believe that the peak at 42.5° – 44.0° corresponds to the nickel-zinc alloy phase. The absence of oxide nickel in spent samples indicates the activity of this form of nickel in reactive desulfurization. Presence of Ni-Zn alloy confirms the assumption of a strong Ni-Zn interaction and its effect on the HDS/HYD selectivity of the process. Apparently, the appearance of this phase prevents the regeneration of nickel by zinc oxide, which is confirmed by the presence of the nickel sulfide phase in the diffraction pattern of the 8-Ni/ZnO-SiO_2 sample. In addition, it is the effect, in our opinion, that explains the low sulfur capacity of Ni/ZnO-SiO_2 system compared to Ni/ZnO-Al_2O_3 one.

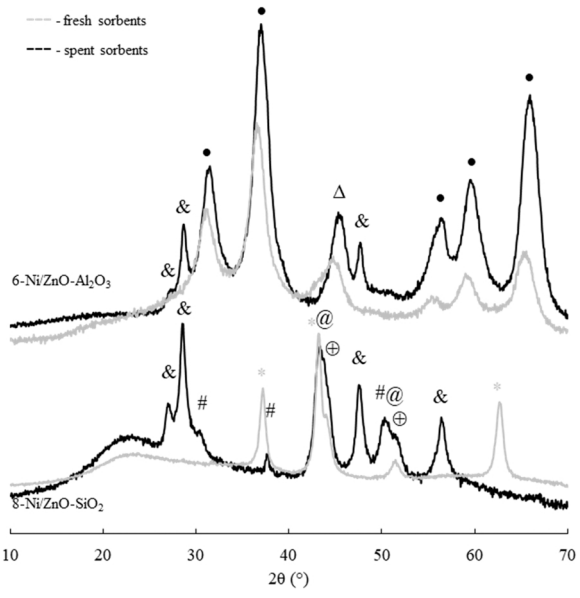

Fig. 10. XRD patterns of spent sorbents. ⊕ – Ni (PDF 04–0850), Δ – γ-Al_2O_3 (PDF 29–0063), • – $ZnAl_2O_4$ (PDF 82–1043), & – ZnS (79–2204), # – Ni_3S_2 (PDF 02–0772), @ - $NiZn_3$ (PDF 47–1019), * – NiO (PDF 78–0429).

3.3. Benchmarking RADS sorbents

The test results are comparable with data reported for RADS (Table 6). HDS activity of adsorbents with the nickel surface concentration of 8 at/nm^2 corresponds to the best reported samples. ZnO-Al_2O_3 systems are much less selective in HDS/HYD than the known RADS sorbents. However, it should be noted that HDS/HYD selectivity for systems based only on alumina has not been discussed in detail in the literature. At the same time, ZnO-SiO_2 adsorbents demonstrated HDS/HYD selectivity values similar to those reported for the model feedstock at a high level of desulfurization activity. The capacity of the synthesized 8-Ni/ZnO-Al_2O_3 and 8-Ni/ZnO-SiO_2 sorbents was relatively higher than the average for alumina/silica-supported sorbents. Higher HDS/HYD selectivities and sulfur capacities communicated in the literature were only achieved during bulk sorbents testing at higher LHSV values or real FCC naphtha desulfurizing in fluidized bed.

3.4. Structure-property analysis in chemisorption and catalysis

The increase in the size of the active phase particles led to the increase in the HDS/HYD selectivity factor of adsorptive-catalytic systems both at the chemisorption and at the catalytic stage (Fig. 11). At the catalytic stage, this effect can be associated with the increased nickel surface concentration, since this correlation could only be traced for each support individually. However, at the chemisorption stage, this correlation was observed for Al_2O_3, ZnO-Al_2O_3 and SiO_2 systems together. This indicated the presence of a size effect, the influence of which exceeded that of the support composition and surface concentration of the active phase.

As noted above, for the RADS process, the influence of active phase particles dispersion on the desulfurization activity of sorbents was previously studied; its effect on HDS/HYD selectivity has not been systematically studied. Therefore, the size effect established by us is also inherent in other FCC desulfurization catalysts, however, for Ni(Zn) systems of the RADS process, it was discovered for the first time. According to the data obtained, it can be seen that the systems supported by ZnO-SiO_2 demonstrate high selectivity, which is not explained only by the average particle size of the active phase. Obviously, there is another effect that provides a significant decrease in the hydrogenating activity of sorbents at the stage of chemisorption. In our opinion, such an influence can be exerted by a strong Ni-Zn interaction between the active phase and free ZnO, which is present on the surface of Ni/ZnO-SiO_2 samples. It is known from the literature that such an interaction can reduce the hydrogenating activity of catalysts, for example, in methanation processes [43]. Therefore, we believe that this is the reason for the significant HDS/HYD selectivity of Ni/ZnO-SiO_2 systems.

Zinc oxide also has a decisive influence on the change in activity and HDS/HYD selectivity factor of sorbents after nickel sulfidation (catalysis regime). For Ni/Al_2O_3 and Ni/SiO_2 sorbents, an increase in the HDS/HYD selectivity factor during nickel sulfidation in feed stream can be noticed (Figs. S11-S13). This is due to the lower activity of nickel sulfide in olefin hydrogenation, while HDS and HYD decrease linearly correlates with the active phase average particle size (Figs. S14 and S15). For nickel particles, such a correlation has not been reported before. On the other hand, for Ni/ZnO-Al_2O_3 and Ni/ZnO-SiO_2 samples, the HDS/HYD selectivity factor at the chemisorption stage is higher than that at the catalytic stage. At the same time, HDS and HYD decrease does not correlate with the average particle size. It can be assumed that this is due to the retention of metallic nickel in the composition of the samples due to the Ni-Zn interaction, which prevents the sulfidation of the active phase. In addition, the high HDS/HYD selectivity factor of the Ni/ZnO-

Table 6
Comparison of obtained data with results of reported RADS studies.

Sorbent	Ref.	Feed, sulfur content	T (°C)	P_{H2} (MPa)	LHSV/ WHSV (h^{-1})	HDS (%)	HYD (%)	SF	Capacity mg_S/g_{Me} [a]
8-Ni(10.2%)/ ZnO-Al_2O_3	Curr.	Model 1000 ppm	400	0.5	5.2	95.5	95.8	0.98	103.7
8-Ni(14.1%)/ ZnO-SiO_2	Curr.	Model 1000 ppm	400	0.5	5.2	95.8	42.9	5.66	46.4
Cu/ZnO	[38]		300	1.0	2	60.0	24.0	3.34	84.8
Ni/ZnO- Al_2O_3−SiO_2	[19]	Model 3500 ppm	390	1.0	11.4	99.7	–	–	–
Ni (20%)/ZnO	[39]	Model 100 ppm	400	1	60	100.0	36	15.48	382.4
Ni (14%)/ ZnO-SiO_2-Al_2O_3	[40]	FCC naphtha 525 ppm	370	2	7.6 Fluidized bed	99.8	32.4	15.87	163.4
Ni-ZnO/Al_2O_3-Diatomite	[41]	Model 2000 ppm	400	1	4	95.0	35.8	6.76	20.1
Ni (9.1%)Pb/ZnO-diatomite-ZSM-5	[42]	Model naphtha 220.4 ppm	425	0.5	3	97.7	84.4	2.03	18.7

[a] Capacity is the ratio of the mass of sulfur adsorbed to the mass of nickel, copper, lead, and zinc.

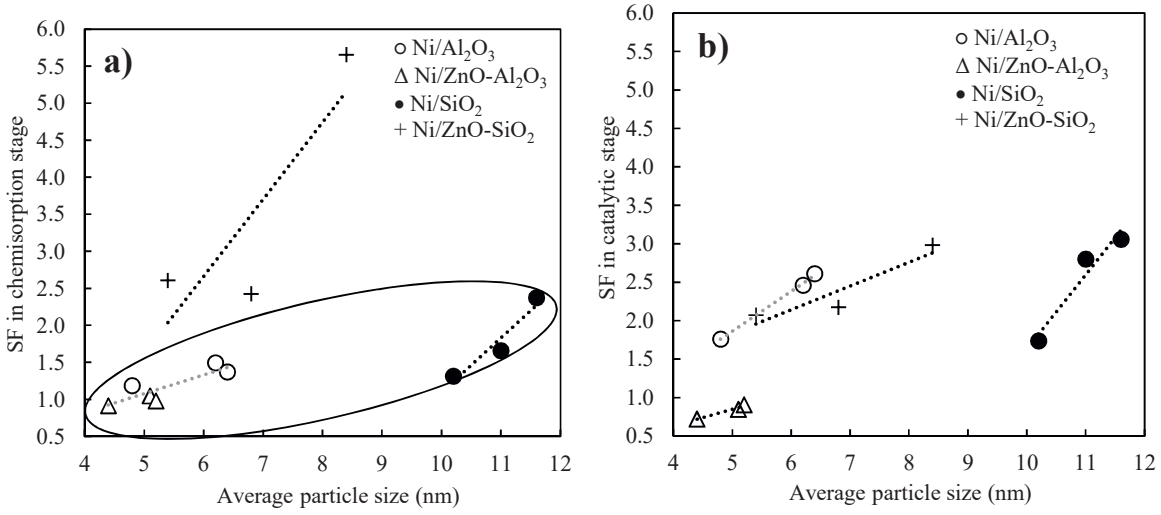

Fig. 11. Relationship between SF and average particle size for the chemisorption stage (a) and catalytic stage (b).

SiO_2 systems at chemisorption stage can be explained by the presence of free zinc oxide. Apparently, since the zinc oxide is converted to zinc sulfide, this effect disappears, resulting in a decrease in selectivity.

The influence of Ni particles dispersion on the TOF number in thiophene and 1-hexene reactions is demonstrated in Fig. 12. It is clearly seen that with the increase of dispersion the TOF number increases both for thiophene and 1-hexene transformations, and the obtained data is best described by the exponential dependence. The large scatter of the values relative to the curves can be due to a large difference between the chemical composition of the samples (SiO_2 and Al_2O_3).

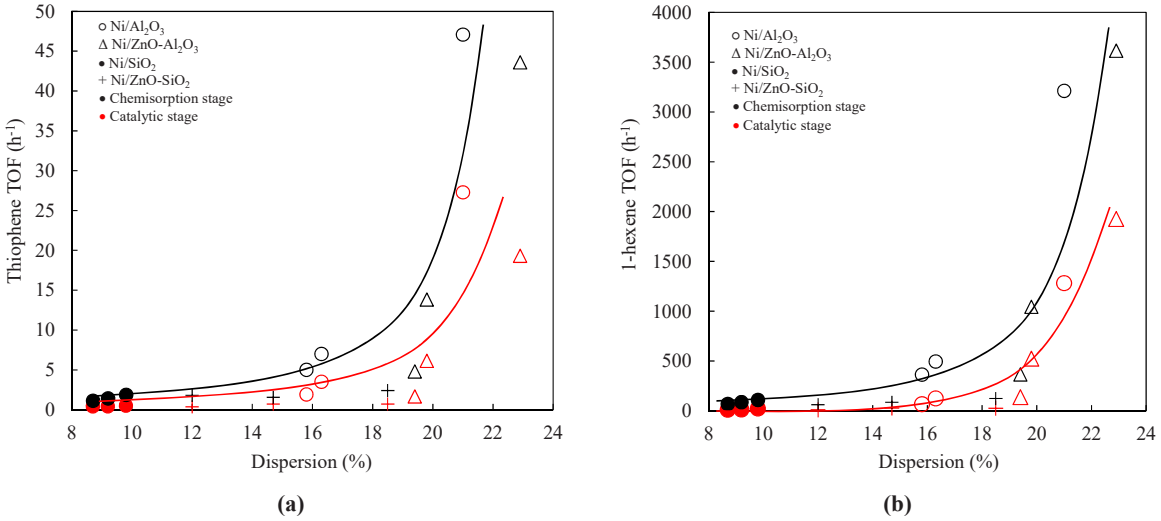

Fig. 12. Relationship between the thiophene TOF number and dispersion of active phase species for thiophene HDS (a) and for 1-hexene HYD (b) reactions.

When calculating TOF from Eqs. (5) and (6), it was assumed that the reduced form of nickel on the surface of active particles acts as the active phase in the reaction with thiophene and olefins. The TOF calculation results are shown in Fig. 12. It is seen that with the increase of Ni particles dispersion the TOF number increases both for thiophene HDS and for 1-hexene HYD reactions. In addition, the TOF dependences from nickel dispersion for chemisorption and catalytic stages are similar, which indicates the prevailing effect of the dispersion parameter on TOF of the reactants rather than the effect of sulfur saturation of the Ni sorbent.

However, it is reasonable to consider another approach to the TOF calculation of reactants at the catalytic stage of the experiment. It is possible to regenerate surface sulfided nickel with oxide nickel with increasing the sulfurization depth at the end of the chemisorption stage. Therefore, TOF values were also estimated for the catalytic stage without taking into account the metallic nickel fraction (Figs. S16 and S17). The resulting data confirms the increase in thiophene HDS and the 1-hexene HYD TOF number with increasing nickel particles dispersion. Based on the results of the studies, there are several factors affecting HDS/HYD selectivity of adsorptive-catalytic systems. The increase in the surface concentration of nickel leads to the increase in HDS/HYD selectivity both at the chemisorption and at the catalytic stage. The decrease in dispersion of active phase particles has a predominant effect on the increase in HDS/HYD selectivity. Interaction between ZnO and Ni determines high HDS/HYD selectivity at the chemisorption stage of $ZnO\text{-}SiO_2$ systems.

3.5. DFT calculation results

To further explore the influence of the surface concentration of nickel, adsorption thermodynamics of three model feedstock components were studied for a series of nickel clusters. As a result, adsorption selectivity of the sulfur-containing compound was calculated in equilibrium conditions. An attempt was also made to address the energetics of adsorption in the diffusion-controlled mode. For this purpose, we postulated that the adsorption favorability under these conditions could be estimated from enthalpies of all probable structures. This treatment explicitly takes into account the possibility that guest molecules have many different configurations. Evidently, the less favorable adsorbate structures undergo conformational changes to the most favorable

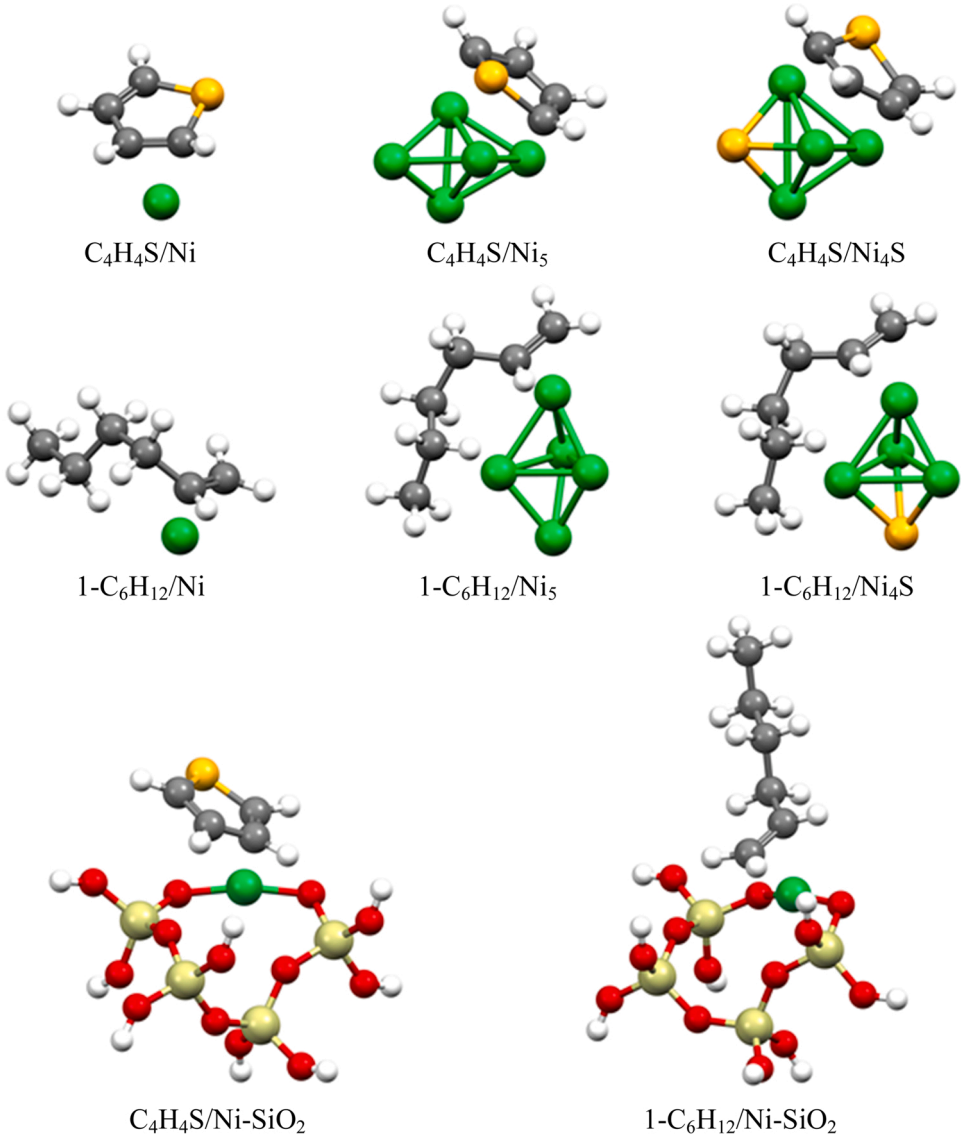

Fig. 13. Exothermic adsorption geometries of thiophene and 1-hexene at selected Ni, Ni_5, Ni_4S, $Ni\text{-}SiO_2$, Ni-ZnO, and $Ni\text{-}Al_2O_3$ clusters, where green, gray, white, orange, pink, purple, red, and yellow balls represent nickel, carbon, hydrogen, sulfur, aluminum, zinc, oxygen, and silicon atoms, respectively (please see the online version for the colors).

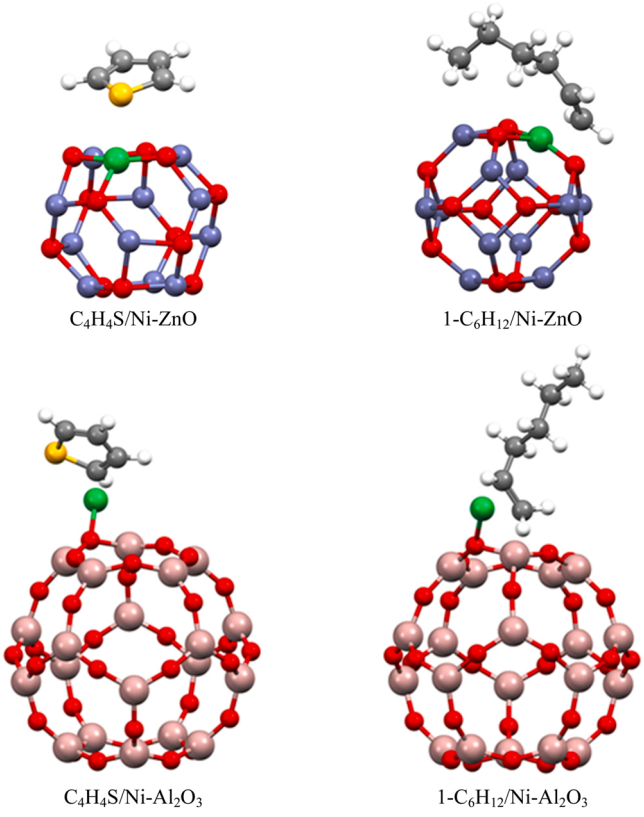

Fig. 13. (*continued*).

adsorption adducts when the conditions are controlled by thermodynamics.

In total, 214 structures (50 for thiophene, 44 for n-heptane, and 120 for 1-hexene) were optimized successfully as viable adsorption adducts. The optimized structures encompassed various modes, including the η^1(S), η^2, η^4, and η^5 configurations. Fig. 13 shows two different molecular geometries optimized for thiophene adsorption on selected pure and sulfided nickel clusters. In theory, both direct desulfurization (DDS) and indirect desulfurization via hydrogenation (HYD) can involve π-complexation or S–M bonding as a control mode during the adsorption step. The π-complexation type was observed in the preferred adsorption modes of thiophene in all nickel clusters under this study. Therefore, the most stable (global optimum) configuration of this mode was selected as the basis for the adsorption selectivity studies under thermodynamically controlled conditions. Furthermore, we note that curled up structures are in most cases preferable for the most stable configurations of 1-hexene and n-heptane.

Interactions of thiophene with Ni_x ($x = 1$–5) clusters could be categorized as strong chemisorption with the enthalpy varying from 47.65 kcal/mol (Ni_2) to 82.49 kcal/mol (Ni_5). In a relevant study, Zhu et al. [44] found that thiophene adsorption was more favorable on Ni_{55} cluster than on Ni(111) surface. Putting these findings together lets someone to contemplate that there should be an optimum limit for increasing the Ni cluster size on every support in terms of desulfurization favorability. The authors did not report the competitive adsorption of feedstock components on different nickel clusters or the effect of nickel sulfidation, as addressed in our study. Based on thermochemical data, thiophene was adsorbed more strongly than n-heptane in all nickel structures. However, this advantage was insignificant for Ni and NiS active sites. Moreover, adsorption of 1-hexene was favored on monatomic and diatomic sites indicating its high propensity for facilitating subsequent HYD reactions.

Selectivity factors for the adsorption competition relative to 1-hexene and n-heptane were evaluated based on Gibbs free energy calculations using the expressions $S_O = K_{Th}/K_{Hex}$ and $S_P = K_{Th}/K_{Hep}$ where K represents the adsorption equilibrium constant and O and P subscripts refer to olefin and paraffin molecules, respectively. The former ratio was used as an indicator of the HDS/HYD favorability in this case. By analogy, selectivity with respect to the equimolar mixture of n-heptane and 1-hexene as feedstock (S_M) was also calculated. The results are shown in Fig. 14.

Selectivity data given herein show that a higher surface concentration of Ni atoms per thiophene molecule can provide higher selectivity values with respect to both thiophene/n-heptane and thiophene/1-hexene favorability. In both thermodynamic and diffusion modes, an upward selectivity trend with the Ni cluster size was observed. Interestingly, thiophene/olefin selectivity approached that of thiophene/paraffin at larger clusters, particularly under diffusion-controlled conditions. Simultaneously, monatomic and diatomic nickel species exhibited unsatisfactory thiophene/1-hexene selectivity, which let conclude that these active sites were not suitable in terms of the HDS/HYD activity ratio.

A net charge transfer of 0.277–0.546 e occurred from the Ni substrate to the thiophene molecule. Nonetheless, our Bader charge analysis predicted no significant correlation between the charge transfer and the adsorption strength. Fig. 15 shows partial densities of states (PDOS) for selected thiophene adsorption adducts. As evident, the HOMO–LUMO energy gap of the adsorption structure decreased from 3.86 to 2.03 eV upon increasing the cluster size. Although the d-PDOS peak was sharp, a decrease in intensity was observed in the case of the Th/Ni_5 adduct. At the same time, the sharp peak of the PDOS for the d-orbitals experienced a shift away from the HOMO energy level upon adsorption of thiophene on both Ni and Ni_5 substrates, with the deviations –0.13 and −0.16 eV, respectively. For comparison, corresponding d-band shifts on the same active sites were calculated to be –0.09 and + 0.17 eV after 1-hexene adsorption. The changes in the electronic structure highlight the role of the quantum effect of the nickel surface concentration and corroborate the energy findings mentioned earlier.

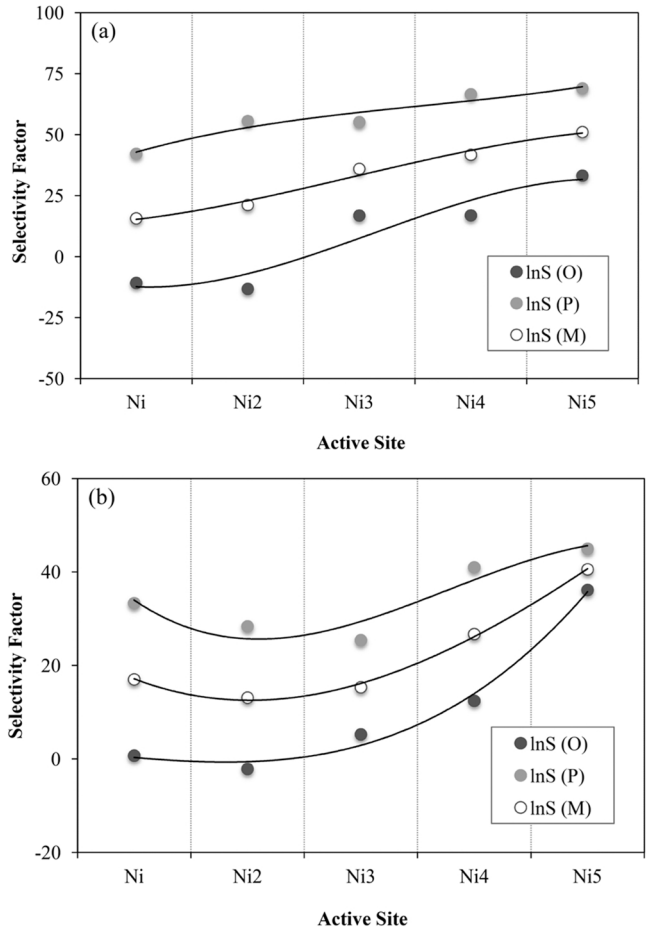

Fig. 14. Changes in selectivity of thiophene adsorption with respect to olefin (O) and paraffin (P) molecules and their equimolar mixture (M) under (a) thermodynamic and (b) diffusion-controlled conditions.

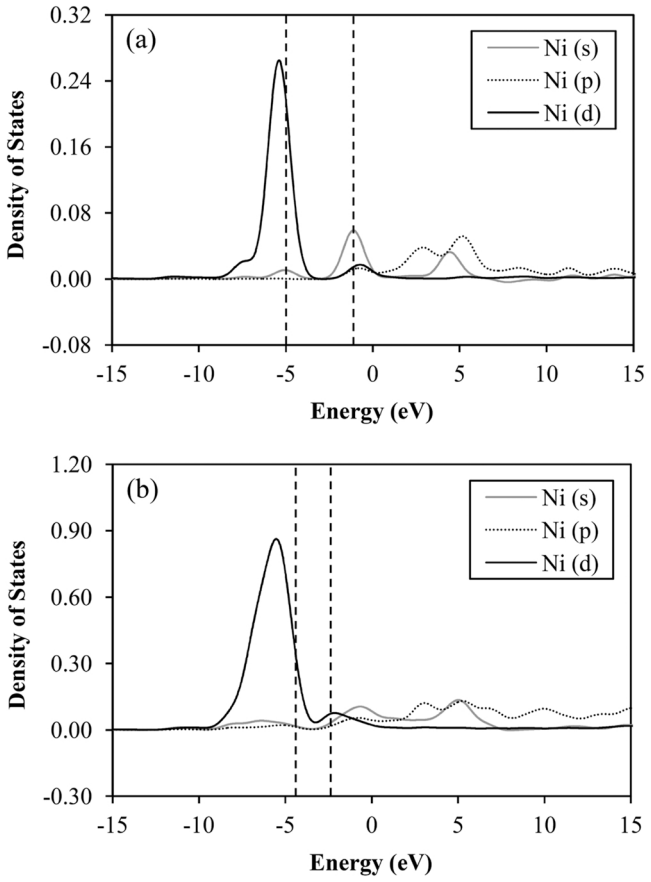

Fig. 15. Partial densities of states (PDOS) of nickel for the highest adsorption energy configurations of thiophene on (a) Ni and (b) Ni5 clusters. The area between the vertical dashed lines indicates the HOMO–LUMO energy gap.

We also used $NiSi_4O_{13}H_8$ [45,46], $NiZn_{11}O_{12}$ [47], and $NiAl_{20}O_{30}$ [48] cluster models to simulate the adsorption of thiophene and 1-hexene on Ni-SiO_2, Ni-ZnO, and Ni-Al_2O_3 at M06/TZVP//M06/SVP in order to further investigate the effect of support. These models represent supported catalysts containing single-atom active sites with nickel contents comparable to the experimental samples. The logarithmic value for desulfurization selectivity with respect to olefin ($\ln S_O$) followed the sequence of Ni (–10.72) < Ni-ZnO (–10.40) < Ni-SiO_2 (–9.74) < Ni-Al_2O_3 (–5.24) < Ni_5 (33.20). As evident, the use of support led to only a slight improvement in single-atom catalysis in terms of adsorption selectivity. At the same time, we note that supported catalysts can provide higher desulfurization activity and sulfur transfer capacity compared to unsupported samples thanks to enhanced dispersion of active metal [19]. Moreover, the influence of support on facilitating sulfur transfer or the formation and desorption of H_2S and butadiene is outside the scope of this work and would be interesting to study at a later stage. In full correspondence with the above findings, these results indicated that too low nickel concentrations disfavor the adsorption selectivity compared to larger clusters. Especially fully substituted active sites are often in high oxidation states that are not readily reducible. Further computations are required to unequivocally shed light on different aspects of desulfurization steps on every supported catalyst.

Sulfided nickel clusters represent partially reduced active species formed in the course of reactions. The selectivity calculations of these clusters indicated that the impact of cluster size at the molecular scale was more pronounced than the role of sulfurization. As a result, the overall selectivity trends in both reaction modes remained more or less the same after sulfurization of the Ni surface, which was confirmed by the TOF calculations. Specifically, these calculations have not confirmed the importance of sulfur in terms of higher adsorption selectivity. However, as the sulfur-metal binding energy (EMS) for the Ni–S bond increased monotonically from NiS (125.32 kcal/mol) to Ni_7S (190.30 kcal/mol), we can pinpoint that excessively large Ni_xS clusters may require more stringent catalyst regeneration conditions. This counteracting trend suggests the possibility of optimizing the surface concentration for optimized HDS/HYD activity with this descriptor by adjusting both Ni loading and dispersion on each support, as discussed in the experimental section (Table 5, Fig. 11).

4. Conclusion

The process of reactive adsorption desulfurization of model FCC gasoline on a series of Ni/ZnO-Al_2O_3 and Ni/ZnO-SiO_2 sorbents with the surface concentration of nickel atoms of 2, 6 and 8 Ni at/nm^2 was studied. Using XRD, TPR, HRTEM and XPS techniques, it was found that the prepared alumina and silica-based sorbents differed significantly in the average particle size of the active phase (4.4–6.4 nm and 5.4–11.6 nm, respectively) and the amount of metallic nickel on the surface after reduction (1.3–10.4% and 29.8–49.5%, respectively). It was found that zinc oxide affected the active phase properties differently depending on the type of the support and interaction with it. On the surface of alumina, zinc oxide was in a bound state. Therefore, Al_2O_3 and ZnO-Al_2O_3 systems had similar Ni dispersion values (15.8–21.0% and 19.4–22.9%, respectively) and the state of surface nickel atoms. In the case of silica, zinc oxide was not bound to the support and was more active, which led to its interaction with the Ni active phase and

significantly raised the position of the main TPR peak maximum (100–230 °C shift) and approximately twofold enhanced dispersion of Ni particles.

It was found that the increase in Ni loading from 2 to 8 at/nm^2 led to the increase in HDS and HYD performance, as well as in the HDS/HYD selectivity factor of adsorptive-catalytic systems both at the chemisorption and at the catalysis stage after sulfur saturation from the feed. The relationship between the HDS/HYD selectivity factor of Ni-based sorbents and size of active phase particles was shown. Using DFT calculations, adsorption geometries and enthalpies of thiophene, 1-hexene and n-heptane on metallic (Ni_1-Ni_5) and sulfided (Ni_1S-Ni_5S) clusters were determined. The DFT calculations confirmed that the HDS/HYD selectivity factor of Ni active sites increases when dispersion of nickel decreases both for metallic and sulfide states.

The effect of zinc oxide on the HDS/HYD selectivity factor of sorbents at the chemisorption stage is of interest. For Al_2O_3-based systems, the presence of zinc oxide led to the decrease in HDS/HYD selectivity and the reverse situation was observed for SiO_2-based systems due to beneficial Ni-Zn interaction and satisfactory dispersion of the active phase. The 8-Ni/ZnO-SiO_2 sample with high Ni loading (8 at Ni/nm^2) exhibited the highest HDS/HYD selectivity factor equal to 5.66 at a high level of thiophene conversion (96%).

CRediT authorship contribution statement

A.A. Botin: Investigation, Writing – original draft. **R.E. Boldushevskii:** Formal analysis, Validation. **A.V. Mozhaev:** Investigation, Visualization, Resources. **M. Ghambarian:** Investigation, Methodology, Writing – original draft. **M. Balar:** Investigation, Validation. **M. Ghashghaee:** Supervision, Project administration, Writing – review & editing. **P.A. Nikulshin:** Supervision, Project administration, Writing – review & editing.

Declaration of Competing Interest

The authors declare that they have no known competing financial interests or personal relationships that could have appeared to influence the work reported in this paper.

Data Availability

Data will be made available on request.

Acknowledgments

The work was funded by RFBR and INSF, project numbers 20-58-56019 and 99003824.

Appendix A. Supporting information

Supplementary data associated with this article can be found in the online version at doi:10.1016/j.apcatb.2023.122946.

References

[1] U.S. Energy Information Administration, "International Energy Outlook", can be found under ⟨https://www.eia.gov/outlooks/ieo/,2021⟩, (accessed Oct. 2022).
[2] U.N. Environment Program, "The global sulfur progress tracker", can be found under ⟨https://www.unenvironment.org/resources/toolkitsmanuals-and-guides/global-sulfur-progress-tracker,2020⟩ (accessed Sep. 2022).
[3] V.C. Srivastava, An evaluation of desulfurization technologies for sulfur removal from liquid fuels, RSC Adv. 2.3 (2012) 759–783, https://doi.org/10.1039/C1RA00309G.
[4] C. Song, An overview of new approaches to deep desulfurization for ultra-clean gasoline, diesel fuel and jet fuel, Catal. Today 86.1–4 (2003) 211–263, https://doi.org/10.1016/S0920-5861(03)00412-7.
[5] R. Abro, A.A. Abdeltawab, S.S. Al-Deyab, G. Yu, A.B. Qazi, S. Gao, X. Chen, A review of extractive desulfurization of fuel oils using ionic liquids, RSC Adv. 4.67 (2014) 35302–35317, https://doi.org/10.1039/C4RA03478C.
[6] B. Saha, S. Vedachalam, A.K. Dalai, Review on recent advances in adsorptive desulfurization, Fuel Process. Technol. 214 (2021), 106685, https://doi.org/10.1016/j.fuproc.2020.106685.
[7] M.N. Hossain, H.C. Park, H.S. Choi, A comprehensive review on catalytic oxidative desulfurization of liquid fuel oil, Catalysts 9 (2019) 229, https://doi.org/10.3390/catal9030229.
[8] S. Brunet, D. Mey, G. Pérot, C. Bouchy, F. Diehl, On the hydrodesulfurization of FCC gasoline: a review, Appl. Catal. A: Gen. 278 (2005) 143–172, https://doi.org/10.1016/j.apcata.2004.10.012.
[9] G. Wang, Y. Wen, J. Fan, C. Xu, J. Gao, Reactive characteristics and adsorption heat of Ni/ZnO–SiO2–Al2O3 adsorbent by reactive adsorption desulfurization, Ind. Eng. Chem. Res. 50 (2011) 12449–12459, https://doi.org/10.1021/ie201144u.
[10] I. Bezverkhyy, G. Gadacz, J.P. Bellat, Interaction of Ni/SiO_2 with thiophene, Mater. Chem. Phys. 114 (2009) 897–901, https://doi.org/10.1016/j.matchemphys.2008.10.058.
[11] I. Bezverkhyy, A. Ryzhikov, G. Gadacz, J.P. Bellat, Kinetics of thiophene reactive adsorption on Ni/SiO2 and Ni/ZnO, Catal. Today 130 (2008) 199–205, https://doi.org/10.1016/j.cattod.2007.06.038.
[12] A. Ryzhikov, I. Bezverkhyy, J.P. Bellat, Reactive adsorption of thiophene on Ni/ZnO: role of hydrogen pretreatment and nature of the rate determining step, Appl. Catal. B: Environ. 84 (2008) 766–772, https://doi.org/10.1016/j.apcatb.2008.06.009.
[13] K. Tawara, T. Nishimura, H. Iwanami, T. Nishimoto, T. Hasuike, New hydrodesulfurization catalyst for petroleum-fed fuel cell vehicles and cogenerations, Ind. Eng. Chem. Res. 40 (2001) 2367–2370, https://doi.org/10.1021/ie000453c.
[14] L. Zhao, Y. Chen, J. Gao, Y. Chen, Desulfurization mechanism of FCC gasoline: a review, Front. Chem. Sci. Eng. 4 (2010) 314–321, https://doi.org/10.1007/s11705-009-0271-9.
[15] F. Ju, L. Li, T. Wu, Y. Sun, H. Ling, Competition between reactive adsorption desulfurization and olefin hydrogenation over the NiO/ZnO–Al2O3–SiO2 adsorbent, N. J. Chem. 46 (2022) 8144–8151, https://doi.org/10.1039/D2NJ01050J.
[16] F. Ju, C. Liu, K. Li, C. Meng, S. Gao, H. Ling, Reactive adsorption desulfurization of fluidized catalytically cracked (FCC) gasoline over a Ca-doped Ni-ZnO/Al2O3–SiO2 adsorbent, Energy Fuels 30 (2016) 6688–6697.
[17] Y. Liu, H. Wang, J. Zhao, Y. Liu, C. Liu, Ultra-deep desulfurization by reactive adsorption desulfurization on copper-based catalysts, J. Energy Chem. 29 (2019) 8–16, https://doi.org/10.1016/j.jechem.2018.01.016.
[18] J. Zhao, L. Zhang, N. She, Y. Liu, Y. Chai, C. Liu, Interaction between Ni and HZSM-5 in aromatization-enhanced reactive adsorption desulfurization catalysts for FCC gasoline upgrading, Appl. Petrochem. Res 4 (2014) 359–365, https://doi.org/10.1007/s13203- 014-0072-z.
[19] C. Wei-Cheng, Y.U. Xiao-Ling, H. Huan, S. Li, M. Xuan, Effect of mixed oxide support for Ni/ZnO in the reactive adsorption desulfurization, China Pet. Process, Petrochem. Technol. 18 (2016) 11.
[20] X. Meng, H. Huang, H. Weng, L. Shi, Ni/ZnO-based adsorbents supported on Al2O3, SiO2, TiO2, ZrO2: a comparison for desulfurization of model gasoline by reactive adsorption, Bull. Korean Chem. Soc. 33 (2012) 3213–3217.
[21] D. Ishutenko, Y. Anashkin, P. Nikulshin, The effect of carrier in KCoMoS-supported catalysts for hydro-upgrading of model FCC gasoline, Appl. Catal. B: Environ. 259 (2019), 118041, https://doi.org/10.1016/j.apcatb.2019.118041.
[22] A.A. Botin, A.V. Mozhaev, R.E. Boldushevskii, Y.A. Khamzin, P.A. Nikulshin, Effect of surface concentration of nickel on the activity and selectivity of Ni/ZnO-Al2O3 sorbents in reactive–adsorption desulfurization of olefin-containing feedstock, Chem. Technol. Fuels Oils 58 (2022) 275–282, https://doi.org/10.1007/s10553-022-01379-3.
[23] A.A. Botin, A.V. Mozhaev, Y.A. Khamzin, R.E. Boldushevskii, P.A. Nikulshin, Reactive adsorption desulfurization of olefin-containing feedstocks over Ni/ZnO–Al2O3 adsorbents: effects of ZnO–Al2O3 support composition, Pet. Chem. 62 (2022) 621–627, https://doi.org/10.1134/S0965544122050036.
[24] G. Bergeret, P. Gallezot, Particle size and dispersion measurements. (2008).
[25] Y. Zhao, D.G. Truhlar, The M06 suite of density functionals for main group thermochemistry, thermochemical kinetics, noncovalent interactions, excited states, and transition elements: two new functionals and systematic testing of four M06-class functionals and 12 other functionals, Theor. Chem. Acc. 120 (2008) 215–241, https://doi.org/10.1007/s00214-007-0310-x.
[26] W.R. Wadt, P.J. Hay, Ab initio effective core potentials for molecular calculations. Potentials for main group elements Na to Bi, J. Chem. Phys. 82 (1985) 284–298, https://doi.org/10.1063/1.448800.
[27] A. Schäfer, C. Huber, R. Ahlrichs, Fully optimized contracted Gaussian basis sets of triple zeta valence quality for atoms Li to Kr, J. Chem. Phys. 100 (1994) 5829–5835, https://doi.org/10.1063/1.467146.
[28] A. Chikhaoui, M. Ziane, S. Tazibt, S. Bouarab, A. Vega, Unveiling the effects of doping small nickel clusters with a sulfur impurity, Theor. Chem. Acc. 137 (2018) 130, https://doi.org/10.1007/s00214-018-2320-2.
[29] F. Ahmed, E.R. Nixon, The A→X system of Ni2 in argon matrices, J. Chem. Phys. 71 (2008) 3547–3549, https://doi.org/10.1063/1.438750.
[30] B. Bak, D. Christensen, L. Hansen-Nygaard, J. Rastrup-Andersen, The structure of thiophene, J. Mol. Spectrosc. 7 (1961) 58–63, https://doi.org/10.1016/0022-2852(61)90341-1.
[31] M. Valiev, E.J. Bylaska, N. Govind, K. Kowalski, T.P. Straatsma, H.J.J. Van Dam, D. Wang, J. Nieplocha, E. Apra, T.L. Windus, W.A. de Jong, NWChem: A comprehensive and scalable open-source solution for large scale molecular simulations, Comput. Phys. Commun. 181 (2010) 1477–1489, https://doi.org/10.1016/j.cpc.2010.04.018.

[32] C.F. Macrae, I.J. Bruno, J.A. Chisholm, P.R. Edgington, P. McCabe, E. Pidcock, L. Rodriguez-Monge, R. Taylor, J. van de Streek, P.A. Wood, Mercury CSD 2.0 - new features for the visualization and investigation of crystal structures, J. Appl. Crystallogr 41 (2008) 466–470, https://doi.org/10.1107/S0021889807067908.
[33] R.F.W. Bader, The quantum mechanical basis of conceptual chemistry, Mon. Chem. 136 (2005) 819–854, https://doi.org/10.1007/s00706-005-0307-x.
[34] T. Lu, F. Chen, Multiwfn: a multifunctional wavefunction analyzer, J. Comput. Chem. 33 (2012) 580–592.
[35] M. Li, H. Li, F. Jiang, Y. Chu, H. Nie, The relation between morphology of (Co) MoS2 phases and selective hydrodesulfurization for CoMo-catalyst, Catal. Today 149 (2010) 35–39, https://doi.org/10.1016/j.cattod.2009.03.017.
[36] R. Ullah, Z. Zhang, P. Bai, P. Wu, D. Han, U.J. Etim, Z. Yan, One-pot cation–anion double hydrolysis derived Ni/ZnO–Al2O3 absorbent for reactive adsorption desulfurization, Ind. Eng. Chem. Res. 55 (2016) 3751–3758, https://doi.org/10.1021/acs.iecr.5b04421.
[37] R. Ullah, M. Tuzen, Interactions of Ni/ZnO with alumina support and their influence on deep reactive adsorption desulfurization, J. Mol. Liq. 365 (2022), 120082, https://doi.org/10.1016/j.molliq.2022.120082.
[38] Y. Liu, H. Wang, Y. Liu, J. Zhao, C. Liu, Reactive adsorption desulfurization on Cu/ZnO adsorbent: effect of ZnO polarity ratio on selective hydrogenation, Energy Fuels 31 (2017) 9930–9938, https://doi.org/10.1021/acs.energyfuels.7b01935.
[39] A. Kong, Y. Wei, Y. Li, Reactive adsorption desulfurization over a Ni/ZnO adsorbent prepared by homogeneous precipitation, Front. Chem. Sci. Eng. 7 (2013) 170–176, https://doi.org/10.1007/s11705-013-1322-9.
[40] J. Fan, G. Wang, Y. Sun, C. Xu, H. Zhou, G. Zhou, J. Gao, Research on reactive adsorption desulfurization over Ni/ZnO− SiO_2− Al_2O_3 adsorbent in a fixed-fluidized bed reactor, Ind. Eng. Chem. Res. 49 (2010) 8450–8460, https://doi.org/10.1021/ie100923v.
[41] X. Meng, H. Huang, L. Shi, Reactive mechanism and regeneration performance of NiZnO/Al_2O_3-diatomite adsorbent by reactive adsorption desulfurization, Ind. Eng. Chem. Res. 52 (2013) 6092–6100, https://doi.org/10.1021/ie303514y.
[42] K. Zhang, Y. Liu, S. Tian, E. Zhao, J. Zhang, C. Liu, Preparation of bifunctional NiPb/ZnO-diatomite-ZSM-5 catalyst and its reactive adsorption desulfurization coupling aromatization performance in FCC gasoline upgrading process, Fuel 104 (2013) 201–207, https://doi.org/10.1016/j.fuel.2012.08.052.
[43] W. Wang, X. Li, Y. Zhang, R. Zhang, H. Ge, J. Bi, M. Tang, Strong metal–support interactions between Ni and ZnO particles and their effect on the methanation performance of Ni/ZnO, Catal. Sci. Technol. 7 (2017) 4413–4421, https://doi.org/10.1039/C7CY01119A.
[44] H. Zhu, X. Li, N. Shi, X. Ding, Z. Yu, W. Zhao, H. Ren, Y. Pan, Y. Liu, W. Guo, Density functional theory study of thiophene desulfurization and conversion of desulfurization products on the Ni(111) surface and Ni_{55} cluster: implication for the mechanism of reactive adsorption desulfurization over Ni/ZnO catalysts, Catal. Sci. Technol. 11 (2021) 1615–1625, https://doi.org/10.1039/d0cy01523g.
[45] I.S. Chuang, G.E. Maciel, A detailed model of local structure and silanol hydrogen bonding of silica gel surfaces, J. Phys. Chem. B 101 (1997) 3052–3064, https://doi.org/10.1021/jp9629046.
[46] M. Ghambarian, M. Ghashghaee, Z. Azizi, M. Balar, Structural diversity of metallacycle intermediates for ethylene dimerization on heterogeneous NiMCM-41 catalyst: a quantum chemical perspective, Struct. Chem. 30 (2019) 137–150, https://doi.org/10.1007/s11224-018-1184-3.
[47] M. Chen, T.P. Straatsma, Z. Fang, D.A. Dixon, Structural and electronic property study of $(ZnO)_n$, $n \leq 168$: transition from zinc oxide molecular clusters to ultrasmall nanoparticles, // J. Phys. Chem. C. 120 (2016) 20400–20418, https://doi.org/10.1021/acs.jpcc.6b06730.
[48] M. Linnolahti, T.A. Pakkanen, Molecular structures of alumina nanoballs and nanotubes: a theoretical study, Inorg. Chem. 43 (2004) 1184–1189, https://doi.org/10.1021/ic0349353.